LARGE EDDIES IN THE FLOW OVER DUNES

Mohammad Omidyeganeh and Ugo Piomelli
Department of Mechanical and Materials Engineering
Queen's University
Kingston, ON, K7L 3N6, Canada
omidyeganeh@me.queensu.ca; ugo@me.queensu.ca

ABSTRACT

We performed large eddy simulation of the flow over a typical two-dimensional dune geometry at laboratory scale (the Reynolds number based on the average channel height and mean velocity is 18,900). The results are validated with simulations and experiments in the literature. A grid sensitivity analysis showed that simulations require approximately five million grid points to converge flow statistics. Large coherent structures can be observed. Large-scale streamwise vortices with sizes of the order of the flow depth are observed. These structures are generated due to the curvature of the bed, and result in re-organization of the streaky structure in the wall layer. Large horseshoe-like structures are generated as a result of the interaction between spanwise rollers and the wall. As they develop, they are tilted downward and attach to the surface by their tips. This creates the events on the free surface known as "boils" (upwelling motions observed at the water surface). The evolution of these structures towards the surface is illustrated and their signatures are studied in details.

INTRODUCTION

The fluid flow over rough sand beds in rivers has unique dynamics compared with the flows that occur when the bed is flat. Depending on the flow Reynolds number, the most commonly found river-bed formations are ripples and dunes. Ripples have dimensions much smaller than the river depth, while dunes may reach heights of the order of the depth. Ripples do not affect the dynamics of the whole flow depth whereas dunes influence on the turbulent flow as well as the sediment transport at the whole depth. Dune formation may affect navigation, erosion of bridge piles and other structures, as well as dispersion of contaminants (Itakura & Kishi, 1980).

One feature of the flow over dunes that has attracted significant attention is the variety of very large (with size comparable to the river depth) coherent structures that are observed. Among the large events caused by these structures are the "boils" (Best, 2005*a*,*b*) (upwelling motions observed at the water surface, usually when a horizontally oriented vortex attaches to the surface); they play an important role in the sediment transport (Kostaschuk & Church, 1993; Venditti & Bennet, 2000) as these eddies lift up sediments and carry them away from the bed.

The uniqueness of the boils in flows over dunes has been illustrated in laboratory measurements (Müller & Gyr, 1986; Nezu & Nakagawa, 1993; Kadota & Nezu, 1999; Best, 2005*a*,*b*) and field observations (Babakaiff & Hickin, 1996; Best, 2005*b*). However, little is known on the generation and evolution of the coherent flow structures that cause them; several studies show that the structures that cause the boils may be originally loop or horseshoe vortices (Kadota & Nezu, 1999; Müller & Gyr, 1986). In our study we take advantage of the three-dimensional and unsteady information supplied by the LES to investigate in detail, for the first time, the dynamics of the eddies responsible for the boil generation.

Numerical simulations can help to understand the dynamics of these events. Other than numerical simulations using Reynolds-averaged Navier-Stokes equations (RANS) (Yoon & Patel, 1996), which cannot show turbulent structures, a few large eddy simulations (LES) have been reported (Yue *et al.*, 2005; Stoesser *et al.*, 2008; Grigoriadis *et al.*, 2009). In general, the mean flow and second-order statistics were in good agreement with the experiments, but large structures illustrated in the simulations differed greatly between the various simulations, and little attention was paid to near-wall events.

Another feature of interest in these flows, and one that has been studied considerably less frequently, is the near-wall turbulence structure. The near-wall eddies are different than those that occur in other canonical wall-bounded flows and are affected by separation, reattachment, curvature of the bed, and pressure gradient that occur on the upward-sloping surface (the "stoss" side). In the present work, we focus on the dynamics of the large-scale coherent structures to understand their signatures.

PROBLEM FORMULATION

In large-eddy simulations (LES) the velocity field is separated into a resolved (large-scale) and a subgrid (small-scale) field, by a spatial filtering operation (Leonard, 1974). The non-dimensional continuity and Navier-Stokes equations for

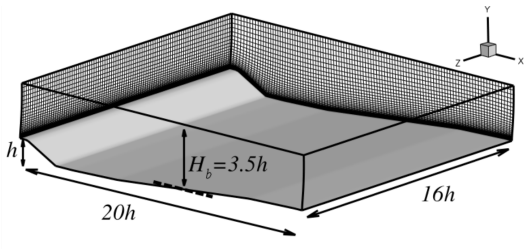

Figure 1. Sketch of the physical configuration. Every fourth grid line is shown.

resolved velocity field are

$$\frac{\partial \overline{u}_i}{\partial x_i} = 0 \quad ; \quad \frac{\partial \overline{u}_i}{\partial t} + \frac{\partial \overline{u}_i \overline{u}_j}{\partial x_j} = -\frac{\partial \overline{P}}{\partial x_i} - \frac{\partial \tau_{ij}}{\partial x_j} + \frac{1}{Re_b}\nabla^2 \overline{u}_i \quad (1)$$

where $Re_b = U_b H_b/\nu$, H_b is the channel average height, and U_b is the average velocity there. Here x_1, x_2 and x_3 are the streamwise, wall-normal and spanwise directions, also referred to as x, y and z. The resolved velocity components in these directions are, respectively, u_1, u_2 and u_3 (or u, v and w); $\tau_{ij} = \overline{u_i u_j} - \overline{u}_i \overline{u}_j$ are the subgrid stresses, which, in the present study, were modelled using an eddy-viscosity assumption

$$\tau_{ij} - \delta_{ij}\tau_{kk}/3 = -2\nu_T \overline{S}_{ij} = -2C\overline{\Delta}^2 |\overline{S}| \overline{S}_{ij}, \quad (2)$$

where $\overline{\Delta} = 2\left(\overline{\Delta x}\,\overline{\Delta y}\,\overline{\Delta z}\right)^{1/3}$ is the filter size, $\overline{S}_{ij} = \left(\partial \overline{u}_i/\partial x_j + \partial \overline{u}_j/\partial x_i\right)/2$ is the resolved strain-rate tensor and $|\overline{S}| = \left(2\overline{S}_{ij}\overline{S}_{ij}\right)^{1/2}$ is its magnitude. The coefficient C was determined using the dynamic model (Germano *et al.*, 1991) with the Lagrangian averaging technique proposed by Meneveau *et al.* (1996), and applied to non-Cartesian geometries by Armenio & Piomelli (2000).

The governing differential equations (1) are discretized on a nonstaggered grid using a curvilinear finite volume code (Silva Lopes & Palma, 2002). The method of Rhie & Chow (1983) is used to avoid pressure oscillations. Both convective and diffusive fluxes are approximated by second-order central differences. A second-order semi-implicit fractional-step procedure (Kim & Moin, 1985) is used for the temporal discretization. The Crank-Nicolson scheme is used for the wall normal diffusive terms, and the Adams-Bashforth scheme is used for all the other terms. Fourier transforms are used to reduce the three-dimensional Poisson equation into a series of two-dimensional Helmholtz equations in wave number space, which are then solved iteratively using the Biconjugate Gradient Stabilized (BCGSTAB) method. The code is parallelized using the MPI message-passing library and the domain-decomposition technique, and has been extensively tested for various turbulent flows (Silva Lopes & Palma, 2002; Silva Lopes *et al.*, 2006; Radhakrishnan *et al.*, 2006, 2008).

Dunes are known to reach a periodic equilibrium shape (Jackson, 1976; Balachandar *et al.*, 2007), with a wavelength equal to 5-6 times the flow depth, and height equal to 1/4 of the flow depth. For this reason, most dune shapes studied experimentally and numerically are quite similar. We use the geometry also used by Balachandar *et al.* (2007) and Stoesser *et al.* (2008). The computational configuration is sketched in Figure 1. Periodic boundary conditions are used in the streamwise (x) and spanwise (z) directions. The flow is driven by a mean pressure gradient, which is assigned in such a way as to maintain the flow-rate constant in time. At the free surface, the wall normal velocity is set to zero, as are the vertical derivatives of the streamwise and spanwise velocity components. In this formulation, the top surface is assumed to be rigid and free of shear stress. Since the surface deformation is expected to be less than 0.5% of the flow depth (Kadota & Nezu, 1999; Yue *et al.*, 2006; Stoesser *et al.*, 2008), the free-slip condition should be accurate. The Reynolds number is $18,900$ based on the channel average height and average velocity at that cross section.

An orthogonal mesh is generated using a hyperbolic grid-generation technique. The resolution of the basic simulation is the same as that used by Stoesser *et al.* (2008) ($416 \times 128 \times 384$ points for a domain twice as wide as that used in the Stoesser *et al.* (2008)), which results in grid spacings in local wall units $\Delta s^+ \approx 12.9$ (streamwise), $\Delta z^+ \approx 6.0$ (spanwise), and $0.1 < \Delta n^+ < 12.1$ (wall normal). Note that the grid spacings above are comparable to those used in many Direct Numerical Simulations of the Navier-Stokes equations. A grid-sensitivity analysis was performed with resolutions of $240 \times 96 \times 200$, $416 \times 128 \times 384$, and $640 \times 180 \times 640$, and grid convergence of the first- and second order statistics was verified: first- and second-order statistics were within 5% of each other for all resolutions. The results obtained with the intermediate grid resolution are shown in the following.

To capture the largest structures in the flow the domain needs to be sufficiently large, especially in the spanwise direction. We initially used a domain with width similar to that used by Stoesser *et al.* (2008), $L_z = 8h$, which is twice as wide as the channel used by Grigoriadis *et al.* (2009). An exam of the spanwise autocorrelation function indicated that an even wider domain ($L_z = 16h$) was necessary to allow the development of the larger eddies at the surface.

RESULTS AND DISCUSSION

The accuracy of the simulations was first verified by a grid-refinement study and by comparing statistics with simulation and experiment reported by Stoesser *et al.* (2008). Figure 2 shows the mean-flow streamlines, and also contours of average (in time and spanwise direction) streamwise velocity, $\langle \overline{u} \rangle$, wall normal velocity, $\langle \overline{v} \rangle$, pressure, $\langle \overline{p} \rangle$, and Reynolds shear stress, $-\langle u'v' \rangle$. The flow separates at the dune crest and reattaches downstream on the bed. Both streamwise and wall normal contours indicate a recirculation region that generates a shear layer. The pressure contours show a favourable pressure gradient that accelerates the flow over the stoss-side (the upward-sloping region for $x > 8h$) and an unfavourable gradient for $x < 8h$. Due to the separation of the flow, a shear layer is generated after the crest that expands in the wake region towards the next dune.

Comparisons between this simulation and the literature, as well as the results of the grid refinement study, are illustrated in Figure 3. The velocities are normalized with the bulk velocity at the last vertical line in 3(a). Good agreement is

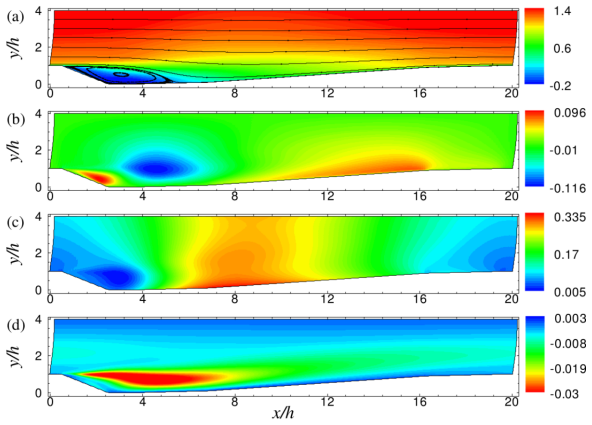

Figure 2. Contour of the average (a) streamwise velocity, $\langle\overline{u}\rangle$, (b) wall normal velocity, $\langle\overline{v}\rangle$, (c) pressure, $\langle\overline{p}\rangle$, and (d) Reynolds shear stress, $-\langle u'v'\rangle$.

obtained with the previous simulation, and between meshes, indicating that the intermediate grid results are fine enough for convergence of statistics. Moreover, as mentioned in the paper by Stoesser *et al.* (2008), the experimental data is not reliable in the wake area due to some inconsistencies in the measurements (mass conservation is not satisfied). Also in Figure 3(c), the Reynolds shear stress is compared along six vertical lines specified in Figure 3(a). Overall good agreement is obtained with experiment and simulation performed by Stoesser *et al.* (2008). As we conclude from the comparison of flow statistics with literature, this simulation could predict the characteristics of the flow over two-dimensional dunes with defined boundary conditions very well.

Turbulence Structure

Figure 4 shows contours of streamwise velocity fluctuations u' on a plane close to the wall, comparing the flow behaviour on the dune with that in an open channel. The latter has the well-known structure of attached wall-bounded flows, with alternating low- and high-speed streaks. The dune shows a rather different behaviour. First, the separation zone on the lee-side of the dune is characterized by large, spanwise-oriented eddies (see, for instance, Le *et al.* (1997)). Secondly, instead of alternating high- and low-speed streaks, we observe streamwise-oriented stripes of low-speed streaks alternated with stripes of high-speed ones. This pattern is due to the presence of large longitudinal vortices on the stoss side of the dune. To visualize these structures, we show, in Figure 5 the secondary-flow streamlines and contours of streamwise velocity fluctuations. These quantities were averaged over a short time, approximately $20h/U_b$, to visualize better the large vortices, which tend to meander. We clearly observe very large structures, of the order of the flow depth. At least two pairs of counter-rotating vortices are observed on average. Similar structures have been observed in experimental and numerical studies of the flow over concave surfaces (Moser & Moin, 1987; Barlow & Johnston, 1988; Lund & Moin, 1996).

The two-point spanwise correlations on the stoss side, shown in Figure 6 for the streamwise and wall-normal velocity components (also averaged over a short time only), also

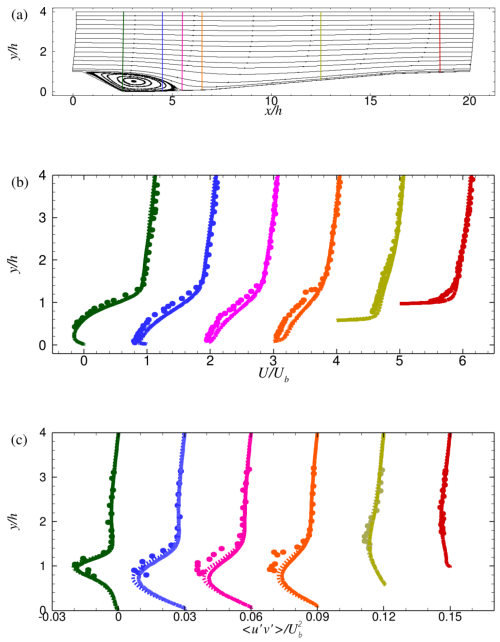

Figure 3. (a) Average streamlines; the vertical lines indicate the position of the profiles in *(b-c)*; (b) streamwise velocity profiles; (c) profiles of Reynolds shear stress; each profile is shifted to the right for clarity. ——— Present simulation, intermediate mesh; — — — present simulation, fine mesh; - - - LES Stoesser *et al.* (2008); • experiment by Polatel cited in Stoesser *et al.* (2008).

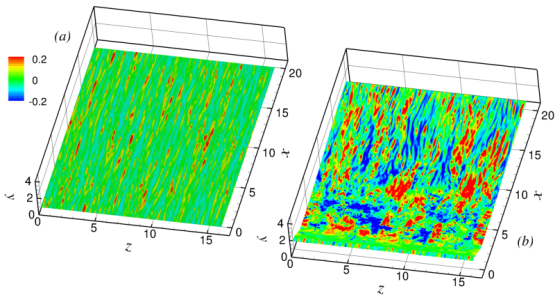

Figure 4. Contours of streamwise velocity fluctuations on a plane parallel to the bed, 5 wall units away from the solid wall. *(a)* Open channel; *(b)* dune.

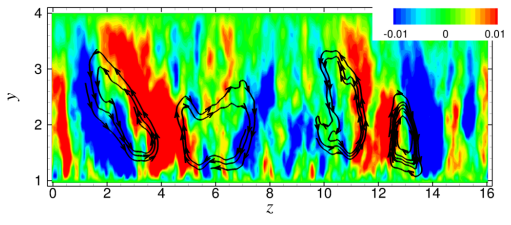

Figure 5. Secondary-flow streamlines in the yz-plane at $x = 15h$, superposed on the contours of short-time averaged wall-normal velocity fluctuations.

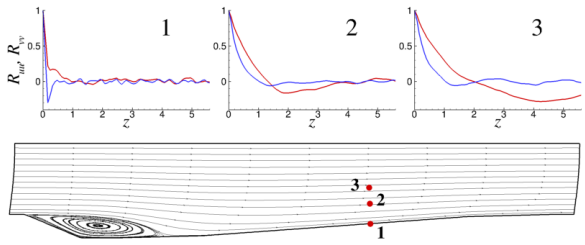

Figure 6. Spanwise auto-correlations at three points on the stoss side. —— R_{uu}; —— R_{vv}.

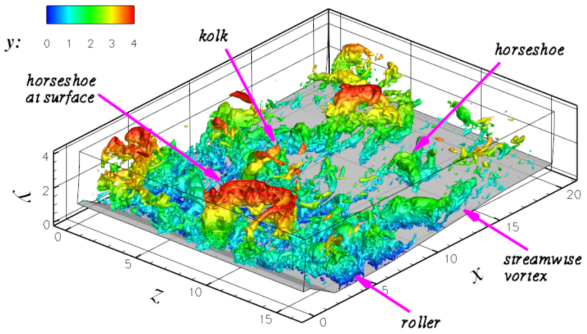

Figure 7. Instantaneous isosurfaces of pressure fluctuation colored with height.

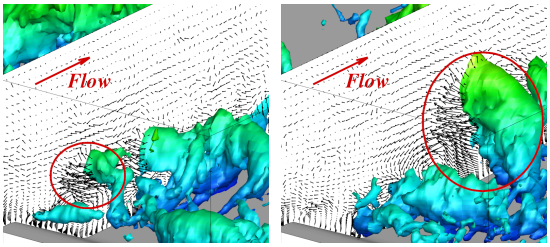

(a) (b)

Figure 8. Evolution of a large horseshoe structure; the time interval between snapshots is $3H_b/U_b$.

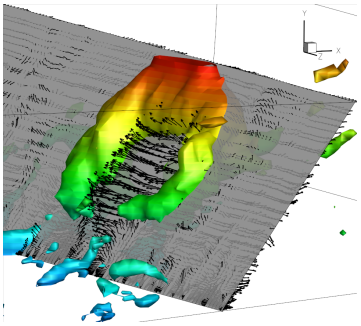

Figure 9. Visualization of the flow near a large horseshoe structure when it touches the surface.

show the signature of these large structures, as well as the streaky structures in the near-wall region. Near the wall R_{vv} has a negative minimum, similar to the canonical boundary layer behaviour. The streamwise-velocity correlation, on the other hand, shows the structure typical of flows with two distinct length scales, with length ration of approximately 4:1. Away from the wall the longitudinal vortices result in a negative peak of the spanwise autocorrelation. The negative peak occurs for a separation $z \sim 4h$, corresponding to the two vortex pairs observed in Figure 5.

Figure 7 shows the outer-layer structures at an instant in time. Rollers (spanwise vortices generated after the separation of flow at the crest) are generated at the crest due to the Kelvin-Helmholtz instability. They are convected downstream and either interact with the near-wall turbulence or rise to the surface. The interaction of rollers near the wall with streamwise vortices generated in the developing boundary layer leads to large horseshoe-like structures. These structures may undergo an intense distortion, become one-legged or be completely destroyed. The region behind the head (and between the legs) of horseshoe vortices is generally characterized by an intense Q2 event (where $u' < 0$ and $v' > 0$), as shown in Figure 8, where the velocity fluctuation vectors in a xy-plane are also shown.

The structure is elongated and tilted downward as it rises to the surface; eventually its tip touches the surface. This development is similar to that observed for horseshoe vortices in open-channel flow over a smooth bed, where Q2 events happen inside the vortex between the legs and Q4 events ($u' > 0$ and $v' < 0$) outside the structure (Adrian, 2007). The vortex is originally vertical (see Figure 8), but is later tilted downward by tip (see Figure 9). The degree of inclination of the structure was measured for several structures of this kind and is between 40^o and 60^o with respect to the $x-z$ plane (Figure 9). The signatures of Q2 and Q4 events are also illustrated by the three-dimensional vectors on the inclined plane in this figure.

As the vortex loop is convected downstream it becomes elongated and distorted. Its legs reach the surface, creating an upwelling, which expands and weakens. Figure 10 shows pressure-fluctuation isosurfaces at four instants. Since the tip of the structure is distorted faster, it is no longer visible with the p' value used. The legs of the vortex loop remain coherent for a longer time, and generate vertical vortices around the boundaries of the boil. This surface behavior was also observed by Best (2005*b*) at larger Reynolds numbers.

As mentioned before, one of the most characteristic events due to coherent structures in the flow over dunes is the appearance of boils, upwelling motions at the water surface. Since in the present calculation the free-surface is rigid, we cannot observe true upwelling motions. We can, however, still identify boil-like events through various surrogate quantities. The first quantity we considered is the pressure: since the boil occurs due to an upward motion, which in this calculation is limited by the rigid surface, we expect boils to be accompanied by significant positive pressure fluctuations p'. Second, the upwelling motion is accompanied by lateral motions; thus, the planar part of the velocity-fluctuation divergence, $\partial u'/\partial x + \partial w'/\partial z$, is expected to be large and positive. The fluctuating velocity vectors, in the free-surface plane, are also expected to be oriented radially from the centre of the boil. Finally, the turbulent kinetic energy (TKE) $\mathscr{K} = \langle u_i' u_i' \rangle / 2$, is expected to be large at the edge of the boil where the flow

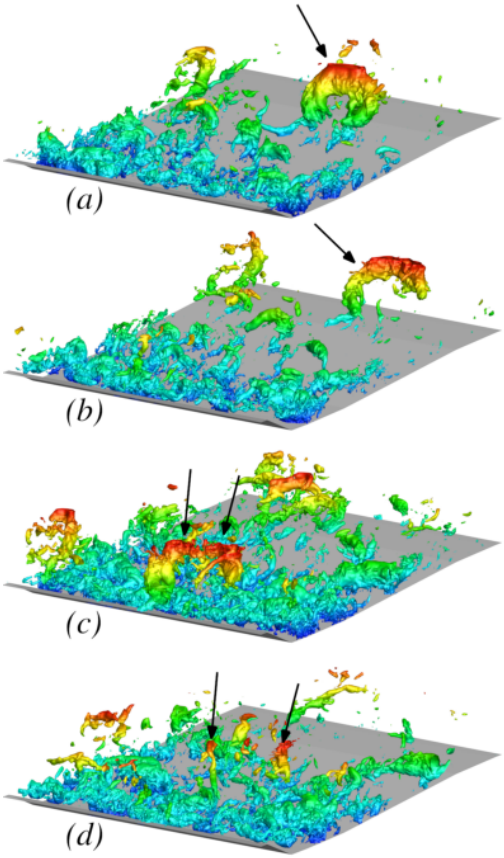

Figure 10. Interaction of the vortex loop with free surface. The time step between snapshots is $3h/U_b$. The horseshoe vortex indicated by an arrow in *(a)* and *(b)* is reintroduced into the domain by the periodic boundary conditions in *(c)* and *(d)*. Pressure isosurface levels are $p' = -0.08$ in *(a)* and *(b)*, -0.06 in *(c)* and -0.04 in *(d)*.

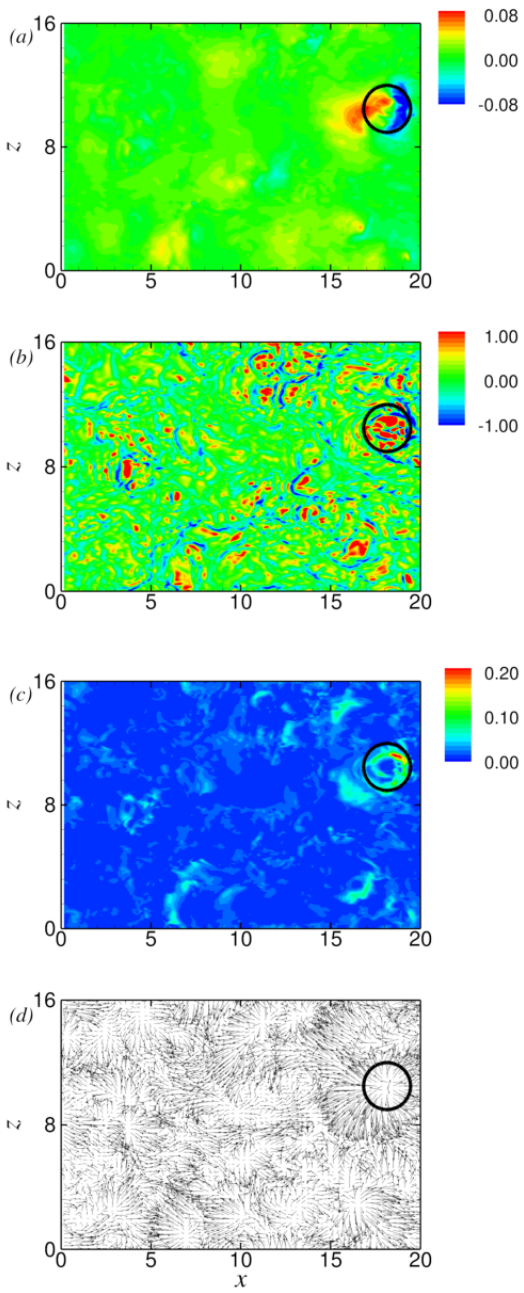

Figure 11. Identification of a boil at the surface of flow over dune bed using *(a)* pressure fluctuations p', *(b)* planar fluctuating velocity divergence $\partial u'/\partial x + \partial w'/\partial z$, *(c)* turbulent kinetic energy $\mathscr{K}$, *(d)* fluctuating velocity vectors.

downdrafts (surface waves in observations by Best (2005*b*)). In Figure 11 we show contours of these quantities on the free surface, at a time corresponding to Figure 10*(b)*. First, we observe a region of negative p' where the head of the horseshoe vortex impinges on the surface. Immediately upstream of the impingement we observe the positive p' region. Consistent with the expected behaviour, we also observe significant values of the planar divergence, large $\mathscr{K}$, and divergence of the velocity vectors. These are the signatures of the boils on the surface. More quantitative analysis is needed in order to quantify these events and compare them with the boils in open channel flow.

CONCLUSIONS

We performed simulations of the flow over two-dimensional dunes at laboratory scale. The effect of the bed form on the turbulence structures is significant. Near-wall structures in the flow over dunes are different than those in an open-channel flow due to the presence of very large streamwise vortices, of the order of the flow depth, that re-organize the streaky structure of the wall layer. There are at least two pairs of counter-rotating vortices similar to the structures have been observed in the flow over concave surfaces. These vortex pairs are separated by $z \sim 4h$. The two-point spanwise correlations near the wall on the stoss side show the signature of these large structures, as well as the streaky structures in the near-wall region.

The main distinction between the structures of the flow over dunes and smooth beds is the presence in the former of

roller structures that interact with wall turbulence, forming an inclined horseshoe-like vortex that is able to reach the surface and make larger and stronger boils, compared with the common boils found in open channel flows. We performed a detailed analysis of the generation and evolution of boils at the surface and showed that the origin of the strong boils in the flow over dunes are the rollers due to Kelvin-Helmholtz instability. The history of these structures shows that they are inclined from their originally vertical orientation, while horseshoe vortices in boundary layer starts from a horizontal orientation. This indicates that these structures are unique to the flow over dunes, in which separation occurs at the crest. It rejects the hypothesis that these structures are originated from the turbulent bursts.

We examined three quantities at the surface to find a reliable identifier for the boils. At the center of the boil, pressure fluctuation is locally high due to the impingement of the flow into the surface. The planar part of the velocity-fluctuation divergence, $\partial u'/\partial x + \partial w'/\partial z$, is large and positive at this point due to the lateral motions. The turbulent kinetic energy is large at the edge of the boil where the flow downdrafts. However, among these signatures, pressure fluctuation is the most robust and reliable identifier.

REFERENCES

Adrian, R. J. 2007 Hairpin vortex organization in wall turbulence. *Phys. Fluids* **19**, 041301.

Armenio, V. & Piomelli, U. 2000 A Lagrangian Mixed Subgrid-Scale Model in Generalized Coordinates. *Flow, Turb. Combust.* **65**, 51–81.

Babakaiff, S. C. & Hickin, E. J. 1996 Coherent flow structures in squamish river estuary, british columbia, canada. In *Coherent Flow Structures in Open Channels* (ed. Phil Ashworth, Sean Bennett, J. L. Best & Stuart McLelland), pp. 321–342. Wiley.

Balachandar, R., Yun, B.-S. & Patel, V. C. 2007 Effect of depth on flow over a fixed dune. *Can. J. Civ. Eng.* **43**, 1587–1599.

Barlow, R. S. & Johnston, J. P. 1988 Structure of a turbulent boundary layer on a concave surface. *J. Fluid Mech.* **191**, 137–176.

Best, J. L. 2005*a* The fluid dynamics of river dunes: A review and some future research directions. *J. Geophys. Res.* **119** (F04S02), 1–21.

Best, J. L. 2005*b* Kinematics, topology and significance of dune-related macroturbulence: some observations from the laboratory and field. In *Fluvial Sedimentology VII* (ed. M. D. Blum, S. B. Marriott & S. Leclair), , vol. 35, pp. 41–60. Spec. Publs. Int. Ass. Sedimentol.

Germano, M., Piomelli, U., Moin, P. & Cabot, W. H. 1991 A dynamic subgrid-scale eddy viscosity model. *Phys. Fluids A* **3**, 1760–1765.

Grigoriadis, D. G. E., Balaras, E. & Dimas, A. A. 2009 Large-eddy simulations of unidirectional water flow over dunes. *J. Geophys. Res.* **114**.

Itakura, T. & Kishi, T. 1980 Open channel flow with suspended sediments. *J. Hydr. Div.* **106** (8), 1325–1343.

Jackson, R. G. 1976 Sedimentological and fluid-dynamic implications of the turbulent bursting phenomenon in geophysical flows. *J. Fluid Mech.* **77**, 531–560.

Kadota, A. & Nezu, I. 1999 Three-dimensional structure of space-time correlation on coherent vortices generated behind dune crests. *J. Hydr. Res.* **37** (1), 59–80.

Kim, J. & Moin, P. 1985 Application of a fractional step method to incompressible Navier-Stokes equations. *J. Comput. Phys.* **59**, 308–323.

Kostaschuk, R. A. & Church, M. A. 1993 Macroturbulence generated by dunes: Fraser River, Canada. *Sedimentary Geology* **85** (1-4), 25–37.

Le, H., Moin, P. & Kim, J. 1997 Direct numerical simulation of turbulent flow over a backward-facing step. *J. Fluid Mech.* **330**, 349–374.

Leonard, A. 1974 Energy cascade in large-eddy simulations of turbulent fluid flows. *Adv. Geophys.* **18A**, 237–248.

Lund, T. S. & Moin, P. 1996 Large-eddy simulation of a concave boundary layer. *Int. J. Heat Fluid Flow* **17**, 290–295.

Meneveau, C., Lund, T. S. & Cabot, W. H. 1996 A Lagrangian dynamic subgrid-scale model of turbulence. *J. Fluid Mech.* **319**, 353–385.

Moser, R. D. & Moin, P. 1987 The effects of curvature in wall-bounded turbulent flows. *J. Fluid Mech.* **175**, 479–510.

Müller, A. & Gyr, A. 1986 On the vortex formation in the mixing layer behind dunes. *J. Hydr. Res.* **24**, 359–375.

Nezu, I. & Nakagawa, H. 1993 *Turbulence in Open-Channel Flows*. Balkema.

Radhakrishnan, S., Piomelli, U. & Keating, A. 2008 Wall-modeled large-eddy simulations of flows with curvature and mild separation. *ASME J. Fluids Eng.* **130** (101203).

Radhakrishnan, S., Piomelli, U., Keating, A. & Silva Lopes, A. 2006 Reynolds-averaged and large-eddy simulations of turbulent non-equilibrium flows. *J. Turbul.* **7** (63), 1–30.

Rhie, C. M. & Chow, W. L. 1983 Numerical study of the turbulent flow past an airfoil with trailing edge separation. *AIAA J.* **21**, 1525–1532.

Silva Lopes, A. & Palma, J. M. L. M. 2002 Simulations of isotropic turbulence using a non-orthogonal grid system. *J. Comput. Phys.* **175** (2), 713–738.

Silva Lopes, A., Piomelli, U. & Palma, J. M. L. M. 2006 Large-eddy simulation of the flow in an S-duct. *J. Turbul.* **7** (11), 1–24.

Stoesser, T., Braun, C., García-Villalba, M. & Rodi, W. 2008 Turbulence structures in flow over two-dimensional dunes. *J. Hydr. Engng* **134** (1), 42–55.

Venditti, J. G. & Bennet, S. J. 2000 Spectral analysis of turbulent flow and suspended sediment transport over dunes. *J. Geophys. Res.* **105**, 22035–22047.

Yoon, J. Y. & Patel, V. C. 1996 Numerical model of turbulent flow over sand dune. *J. Hydr. Engng* **122** (1), 10–18.

Yue, W., Lin, C.L. & Patel, V.C. 2005 Large eddy simulation of turbulent open-channel flow with free surface simulated by level set method. *Phys. Fluids* **17**, 025108.

Yue, W., Lin, C.-L. & Patel, V. C. 2006 Large-eddy simulation of turbulent flow over a fixed two-dimensional dune. *J. Hydr. Engng* **132** (7), 643–651.